Quantum Borrmann effect for dissipation-immune photon-photon correlations

Alexander V. Poshakinskiy and Alexander N. Poddubny*
Ioffe Institute, Sector of quantum coherent phenomena, St. Petersburg 194021, Russia

(Received 2 October 2020; revised 22 January 2021; accepted 7 April 2021; published 26 April 2021)

We study theoretically the second-order correlation function $g^{(2)}(t)$ for photons transmitted through a periodic Bragg-spaced array of superconducting qubits, coupled to a waveguide. We demonstrate that photon bunching and antibunching persist much longer than both radiative and nonradiative lifetimes of a single qubit. Due to the Borrmann effect, that is a strongly non-Markovian collective feature of light-qubit coupling inherent to the Bragg regime, the photon-photon correlations become immune to nonradiative dissipation. This persistence of quantum correlations opens new avenues for enhancing the performance of setups of waveguide quantum electrodynamics.

DOI: 10.1103/PhysRevA.103.043718

I. INTRODUCTION

Cooperative effects are widely used to manipulate light-matter interactions [1,2]. Namely, constructive or destructive interference between light coupled to different resonant emitters can result in enhancement (superradiance) or suppression (subradiance) of the radiative decay rate $\Gamma_{\rm rad}$ as compared with the radiative decay rate of an individual emitter Γ_0. Both super- and subradiant modes have been demonstrated for a variety of experimental platforms, such as resonant plasmonic [3] and dielectric nanostructures [4], solid-state quantum emitters [5,6], individual molecules, etc. For example, long-living supercavity modes with $\Gamma_{\rm rad} \ll \Gamma_0$, inspired by the photonic bound states in the continuum [7], have been recently realized for resonant dielectric nanoparticles [8]. Similar concepts to engineer subradiant modes apply in the quantum regime [9–13] as has been recently demonstrated for single-photon excitations of a superconducting qubit array coupled to a waveguide [14]. It is, however, much harder to suppress the *nonradiative* decay. In the usually valid Markovian regime of light-matter coupling, the nonradiative decay rate $\Gamma_{\rm nonrad}$ just adds an independent contribution to the total decay rate, $\Gamma_{\rm tot} = \Gamma_{\rm rad} + \Gamma_{\rm nonrad}$ that is sensitive neither to the interference nor to the number of emitters. As such, the maximum lifetime $1/(2\Gamma_{\rm tot})$ is given by $t^{(1)}_{\rm nonrad} = 1/(2\Gamma_{\rm nonrad})$, which seems to limit the performance of a real-life quantum system regardless of the sophisticated techniques used to manipulate $\Gamma_{\rm rad}$.

Here, we propose a simple scheme to achieve quantum correlations between photons in an array of superconducting qubits in a waveguide that have the total lifetime much larger that *both* radiative and nonradiative lifetime of an individual qubit. We consider a periodic array of N two-level qubits with the resonant frequency ω_0 and the spacing d, satisfying the resonant Bragg condition

$$d = d_{\rm Bragg} \equiv \lambda(\omega_0)\frac{m}{2}, \quad m = 1, 2, \ldots, \tag{1}$$

where $\lambda(\omega_0) = 2\pi c/\omega_0$ and c is the speed of light, see Fig. 1.

Our proposal is inspired by the Borrmann effect, originally discovered for x-rays [15,16]. The effect manifests itself in anomalous transmission of electromagnetic waves through crystals due to the suppression of absorption in the Bragg regime, when the wave has nodes at the atom centers. Suppression of inelastic channels has also been proposed [17] and studied experimentally for resonant scattering of γ rays on nuclei in crystals, see the review [18]. The Borrmann effect has been also observed in photonic crystals [19], and similar ideas were examined in Bragg arrays of semiconductor quantum wells [20–22], in particular in Refs. [23,24]. The essence of the Borrmann effect can be understood from a properties of the simplest one-dimensional photonic crystal, an array ABABAB ...of alternating layers A and B. Namely, the electric field has nodes centered in layers A at one edge of the photonic band gap and in layers B at the opposite band-gap edge [25]. When layers A (or layers B) acquire complex permittivity, the light absorption appears to be suppressed at the corresponding band-gap edge due to the decrease of the overlap between the electric field and the absorbing layers. Obviously, the effect is greatest when the absorbing layers are subwavelength, as in the case of atoms. However, to the best of our knowledge, the Borrmann effect has never been considered in the quantum structure, which is highly relevant for emerging setups of waveguide quantum electrodynamics based on cold atoms and superconducting qubits [26–30]. While quantum optics for arrays of closely spaced atoms is well developed, implications of Bragg diffraction on the quantum correlations in photonic crystals made of atoms or qubits remain a fundamental problem where much less is understood.

Here we perform a rigorous calculation of the second-order photon-photon correlation function $g^{(2)}(t)$ and demonstrate long-living correlations [$g^{(2)}(t) \neq 1$] of photons transmitted through the Bragg qubit arrays at times $t \gg t^{(1)}_{\rm nonrad}$. The correlations that persist much longer than the *radiative* lifetime are already known for a two-qubit system separated by large anti-Bragg distance $d = (m \pm \frac{1}{2})\lambda_0/2$ [31]. However, the advantage of the current proposal based on the multiqubit Bragg array is that the correlations survive at even longer times, exceeding the *nonradiative* lifetime of a single qubit. This could open new possibilities for applications in quantum

*poddubny@coherent.ioffe.ru

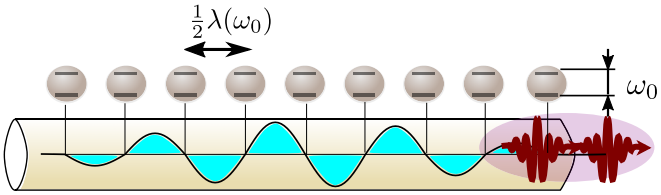

FIG. 1. Schematics of two photons propagating in an array of superconducting qubits coupled to a waveguide and separated by the Bragg spacing $d = d_{\rm Bragg} \equiv \lambda(\omega_0)/2$. Shaded black curve shows the electric field $\mathrm{Re}\, E(z)$ of the most subradiant mode of the nine-qubit array. Calculation parameters are given in the text.

memory and quantum information processing. Our results apply to different platforms of waveguide quantum electrodynamics with superconducting qubits being probably the most suitable one at the moment. Their main advantage is large coupling efficiency of the qubit resonance to the waveguide mode $\beta = \Gamma_0/(\Gamma_0 + \Gamma_{\rm nonrad}) > 99\%$ [29] and the possibility to control each qubit individually, eliminating the inhomogeneous broadening. In the case of a cold atom platform, the coupling efficiency is on the order of $\beta \approx 1\%$ [26,28]. For other platforms, such as quantum defects [32] or quantum dots [33], it is so far relatively hard to produce coherent arrays with more than $N = 2$ qubits due to large inhomogeneous broadening.

II. COMPLEX ENERGY SPECTRUM

We now analyze the energy spectrum of single-excited states of photons coupled to the qubits in a one-dimensional waveguide that will determine the lifetime of photon-photon correlations. The considered structure consists of N periodically spaced qubits and is characterized by the standard quantum-optics Hamiltonian

$$\mathcal{H} = \sum_k \omega_k a_k^\dagger a_k + \sum_j \omega_0 b_j^\dagger b_j + \frac{\chi}{2}\sum_j b_j^\dagger b_j^\dagger b_j b_j + \frac{g}{\sqrt{L}}\sum_{j,k}\left(b_j^\dagger a_k e^{ikz_j} + b_j a_k^\dagger e^{-ikz_j}\right). \quad (2)$$

Here, a_k are the annihilation operators for the waveguide photons with the wave vectors k, frequencies $\omega_k = c|k|$, and velocity c, g is the interaction constant, L is the normalization length, and b_j are the (bosonic) annihilation operators for the qubit excitations with the frequency ω_0 and located at the point z_j. We consider a nonchiral situation, when atoms interact with photons propagating in both directions. The qualitatively different many-body chiral quantum problem has recently been solved in Ref. [34] and the results were experimentally tested in Ref. [35]. In Eq. (2), we consider the general case of anharmonic many-level qubits, the two-level case can be obtained in the limit of large anharmonicity ($\chi \to \infty$) where the multiple occupation is suppressed [31,36]. This procedure is inspired by Abrikosov's approach to spin systems [37]: two states of two-level atom can be mapped to the two states of spin 1/2. The photonic degrees of freedom can be integrated out in Eq. (2), yielding an effective model for light-coupled qubit excitations [11,38],

$$\widetilde{\mathcal{H}} = \sum_{m,n} H_{m,n}(\omega_0) b_m^\dagger b_n + \frac{\chi}{2}\sum_m b_m^\dagger b_m^\dagger b_m b_m, \quad (3)$$

where

$$H_{mn}(\omega) = (\omega_0 - i\Gamma_{\rm nonrad})\delta_{mn} - i\Gamma_0 e^{i\omega|z_m - z_n|/c}, \quad (4)$$

where $m, n = 1, \ldots, N$. The Hamiltonian (4) is non-Hermitian and takes into account the radiative losses characterized by the radiative decay rate for a single qubit $\Gamma_0 = g^2/c$. The interaction between the qubits is long-ranged since it is mediated by the photons propagating in the waveguide. We have also added to the Hamiltonian H_{mn} in Eq. (3) a phenomenological nonradiative decay rate $\Gamma_{\rm nonrad}$ that incorporates all the decay and dephasing mechanisms of the qubits except for emission to the waveguide. In case of atoms coupled to the waveguide, it is mostly associated with the emission into free space [28]. In the case of superconducting qubits, the decoherence can be related to the defects in the Josephson junctions [39]. We also note that, while the distinction between nonradiative decay and pure dephasing can be important for highly excited quantum states, it is less relevant for single-excited subradiant states where they both can be merged in one phenomenological parameter. For example, the non-Hermitian dephasing term $\propto i(b^\dagger b)^2$ for single-excitation systems where $b^\dagger b = 1$ is equivalent to a simpler term $\propto i b^\dagger b$.

The specific procedure of the derivation of the Hamiltonian Eq. (3) starting from Eq. (2) is detailed e.g., in Ref. [38] where the authors use the standard input-output approach of quantum optics. Another rigorous derivation of the equation for single-excited states in the atomic array coupled to a waveguide is presented in Ref. [40] where it is shown that their coupling is described by a classical electromagnetic Green's function. In the case where the coupling is determined only by the guided mode, the problem becomes effectively one dimensional and the three-dimensional (3D) Green's function from Ref. [40] reduces to the one-dimensional (1D) Green's function $e^{i\omega|z_m - z_n|/c}$ entering Eq. (4) as shown in Ref. [41]. An alternative but equivalent derivation is presented in Ref. [12] where we demonstrate that the poles of the two-photon scattering matrix calculated by using the rigorous Green's function technique can be equivalently found from Eq. (3) for single- and two-photon excitations. Specifically, the values of complex eigenfrequencies ω for single-excited states are determined by the positions of the poles of the Green's function, that can be presented in the matrix form as $G(\omega) = [H(\omega) - \omega]^{-1}$, where $H(\omega)$ is the matrix Hamiltonian (4).

Crucially, we do not limit ourselves to the Markovian approximation. In the Markovian approximation it is assumed that the photon-mediated coupling between the qubits is instantaneous, i.e., the flight time of photons through the array is much shorter than all the lifetimes of the collective modes in the system. Technically, it means that $H_{mn}(\omega)$ can be replaced by $H_{mn}(\omega_0)$. When the array is long enough, we need to take into account the retardation effects, described by the dependence of the matrix H_{mn} on the frequency ω via the phase $\omega|m - n|d/c$ gained by light when traveling from the qubit

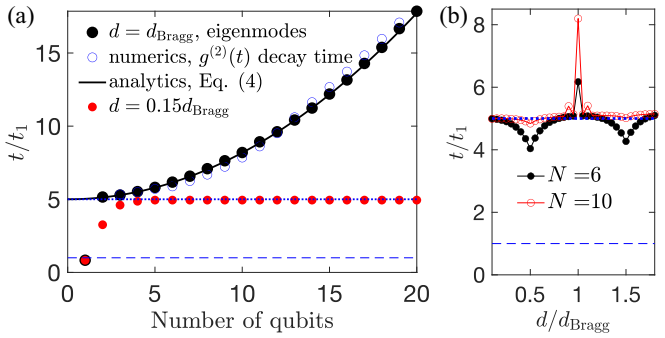

FIG. 2. (a) Numerically calculated lifetime of longest-living eigenmode depending on the number of qubits for a Bragg-spaced array with $\omega_0 d/c = \pi$ (filled black circles) and a short-period metamaterial with $\omega_0 d/c = 0.15\pi$ (small red dots). Solid curve shows the analytical dependence Eq. (5). Open blue circles show the numerically calculated lifetime of the photon-photon correlations $g^{(2)}(t)$. (b) Lifetime dependence on the array period. Black filled and red open circles correspond to $N = 6$ and $N = 10$ qubits. Horizontal blue dotted and dashed lines show the nonradiative and radiative lifetimes for a single qubit, respectively. Calculation has been performed for $\Gamma_{\text{nonrad}} = 0.2\Gamma_0$ and $\Gamma_0/\omega_0 = 10^{-2}$.

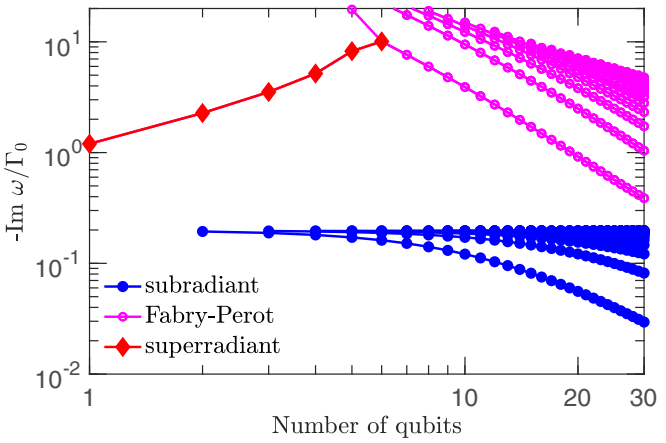

FIG. 3. Decay rates of the complex eigenmodes of the Bragg qubit array depending on the number of qubits N. The calculation parameters are the same as in Fig. 2.

m to the qubit n. The eigenfrequencies are found by solving numerically the equation $\det G^{-1}(\omega) = 0$ for complex ω.

We start by analyzing the lifetime of the longest-living eigenmode $t = 1/(2\min|\operatorname{Im}\omega|)$. Numerically calculated lifetime dependence on the number of qubits N for the Bragg-spaced array is shown by the large black circles in Fig. 2(a). The lifetime greatly exceeds the nonradiative lifetime of a single qubit (blue dotted line). The lifetime dependence is well described by the analytical equation [see Appendix A for derivation details]

$$\frac{t(N)}{t^{(1)}_{\text{nonrad}}} = 1 + \frac{2\Gamma_0}{\omega_0 \pi} N^2, \tag{5}$$

shown by the solid black curve in Fig. 2(a). This quadratic $t(N)$ dependence is very different from the case of short-period array with the spacing defined by $\omega_0 d/c = 0.15\pi$, where the Markovian approximation works well and the lifetime is limited from above by $1/\Gamma_{\text{nonrad}}$, small red circles in Fig. 2(a). The increase of the lifetime in the Bragg case is also seen in Fig. 2(b) where we plot its dependence on the array period for two given numbers of qubits $N = 6$ and $N = 10$. For $N = 6$ the Markovian approximation still works and the lifetime depends weakly on period. However, already for $N = 10$ qubits the lifetime in Bragg structure increases, evincing strongly non-Markovian physics.

Details of the evolution of the complex energy spectrum of the Bragg array with the number of qubits N are examined in Fig. 3. In the Markovian approximation the energy spectrum includes a superradiant mode with $\omega_{\text{SR}} = \omega_0 - i(N\Gamma_0 + \Gamma)$ and $N - 1$ degenerate dark modes, $\omega_{\text{dark}} = \omega_0 - i\Gamma$. Figure 3 shows the evolution of decay rates $-\operatorname{Im}\omega$ of the eigenmodes with increasing N. As a result of the Markovian approximation breaking, the eigenfrequency equation $\det G^{-1}(\omega) = 0$ for the N-qubit system acquires an infinite number of solutions. In addition to the N eigenvalues obtained in the Markovian approximation $H(\omega) = H(\omega_0)$, there exists also an infinite number of generalized Fabry-Pérot eigenmodes whose decay rate decreases with the increase of N. Specifically, at $N = 6 \sim \sqrt{\omega_0/\Gamma_0}$ the superradiant mode (red diamonds) collides with the other mode with $\operatorname{Re}\omega = \omega_0$ and the two modes turn into a pair of generalized Fabry-Pérot modes with the same decay. For large N, the spectrum includes multiple Fabry-Pérot modes (magenta open circles in Fig. 3) and $N - 1$ subradiant modes (small blue dots). More information on the behavior of complex eigenfrequencies of the generalized Fabry-Pérot modes can be found in the following Sec. III A.

Here, we are more interested in the evolution of the subradiant modes. The real parts of their eigenfrequencies are equal to ω_0 and the evolution of the imaginary parts with N is shown in Fig. 3 by small blue dots. When the number of qubits increases the real parts of the complex eigenfrequencies of the subradiant modes stay degenerate and equal to ω_0 but their decay rates, $-\operatorname{Im}\omega$, become different and nonzero. Moreover, imaginary parts of eigenfrequencies are less than Γ_{nonrad} by the absolute value which means that the effective lifetime of the subradiant eigenstates $t = 1/(2|\operatorname{Im}\omega|)$ is longer than both nonradiative and radiative lifetimes of a single qubit. In the limit $N \to \infty$, the complex frequency of the most subradiant mode tends to $\omega = \omega_0$, i.e., the lifetime becomes infinitely long. To understand qualitatively the origin of the long lifetime we plot in Fig. 1 by the shaded black curve the distribution of the electric field, corresponding to the emission from the longest-living eigenmode for $N = 9$ qubits: $E(z) \propto \sum_{m=1}^{N} e^{i\omega|z-md|/c}\psi_m$, where ψ_m is the eigenvector satisfying $H(\omega)\psi = \omega\psi$. The calculated distribution has nodes at the qubit sites, which explains the suppression of the nonradiative decay, similar to the Borrmann effect in the x-ray physics [16]. In another words, the mixed light-qubit polariton wave is almost decoupled from the qubits and absorption is strongly suppressed. Detailed analysis of the energy flow is presented in Sec. III B.

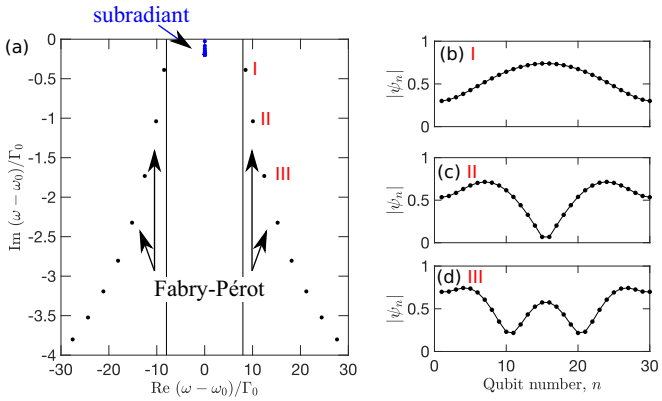

FIG. 4. (a) Energy spectrum of the 30-qubit array showing complex eigenfrequencies of Fabry-Pérot and subradiant modes ω on the complex plane. (b)–(d) Spatial distribution of three lowest Fabry-Pérot modes I–III indicated in panel (a). The calculation has been performed for $\Gamma_{\rm nonrad} = 0.2\Gamma_0$ and $\Gamma_0/\omega_0 = 10^{-2}$.

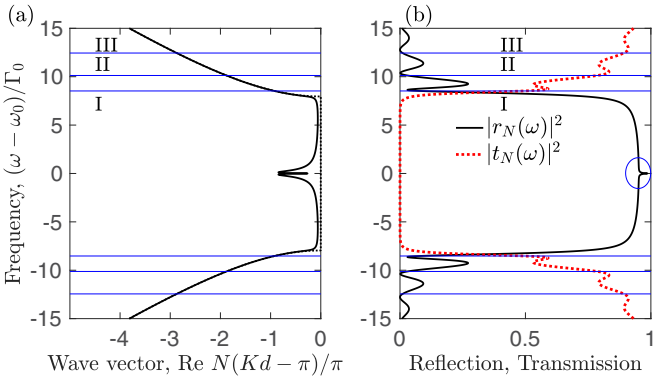

FIG. 5. (a) Dispersion law of exciton-polaritonic modes (A10) for the Bragg 30-qubit array. Dotted and solid curves have been calculated neglecting and including the nonradiative decay, respectively. (b) Reflection and transmission coefficients $|r_N(\omega)|^2$ and $|t_N(\omega)|^2$ calculated from Eqs. (A9). Ellipse indicates the frequency range analyzed in Fig. 9. Calculation has been performed for $\Gamma_{\rm nonrad} = 0.2\Gamma_0$ and $\Gamma_0/\omega_0 = 10^{-2}$. The thin horizontal blue lines I–III show the values of the real parts of the eigenfrequencies of the Fabry-Pérot modes.

III. SUBRADIANT AND FABRY-PÉROT MODES

In this section we provide more details on the identification and behavior of generalized Fabry-Pérot modes (Sec. III A) and subradiant modes (Sec. III B).

A. Generalized Fabry-Pérot modes

Here we examine in more detail the generalized Fabry-Pérot modes of the qubit array.

The complex energy spectrum for $N = 30$ qubits is shown in Fig. 4(a). Figures 4(b)–4(d) show the spatial distribution of the three eigenvectors ψ for the three modes I–III, found from the numerical solution of the generalized eigenproblem $H_{mn}(\omega)\psi_n = \omega\psi_m$. The spatial profile of the eigenmodes resembles a discrete approximation of the standing waves with zero nodes (I), one node (II), and two nodes (III). This confirms our interpretation of these modes as a result of Fabry-Pérot interference. Further confirmation is obtained from Fig. 5(b), where we compare the real parts of the eigenfrequencies for the modes I–III (blue horizontal lines) with the positions of the Fabry-Pérot oscillations of the reflection and transmission coefficients $|r_N|^2$ and $|t_N|^2$. Finally, comparison of the spectral positions of these eigenmodes with the polariton dispersion $Kd(\omega)$ plotted in Fig. 5(a) shows that their real parts satisfy the interference condition

$$N\,\mathrm{Re}\,[K(\omega)d - \pi] = \pi, 2\pi, 3\pi, \ldots. \tag{6}$$

We note that, contrary to the modes of a conventional Fabry-Pérot resonator, the polariton dispersion law $K(\omega)$ in the atomic array considered is a nonlinear function of ω. Hence, our generalized Fabry-Pérot modes given by Eq. (A13) are not equidistant, similarly to Fabry-Pérot modes of bulk exciton-polaritons in finite slabs [42].

Details of the evolution of the complex energy spectrum of the Bragg array with the number of qubits N are examined in Fig. 6. In the Markovian approximation the energy spectrum includes a superradiant mode with $\omega_{\rm SR} = \omega_0 - i(N\Gamma_0 + \Gamma_{\rm nonrad})$ and $N-1$ degenerate dark modes, $\omega_{\rm dark} = \omega_0 - i\Gamma_{\rm nonrad}$ and Fig. 6 shows the evolution of spectrum with increasing N. The trajectory of the superradiant mode in the complex plane is shown by the vertical black line in Fig. 6. At $N = 6 \sim \sqrt{\omega_0/\Gamma_0}$, the structure exhibits a transition from the superradiant regime to the photonic crystal regime [23,24]. Namely, at $N \approx 6$ the superradiant mode collides with the another mode with $\mathrm{Re}\,\omega = \omega_0$ (vertical blue line in Fig. 6). After the collision these two modes split into a pair of Fabry-Pérot modes, that are mirror-symmetric with respect to ω_0. Their trajectories are shown by curved colored lines with arrows in Fig. 6. This transition from superradiant regime to the photonic crystal regime takes place when the flight time of photons through the system $t_{\rm flight} = Nd/c = N\pi/\omega_0$ becomes shorter than the lifetime of the superradiant mode $1/N\Gamma_0$. For structures with $N \gtrsim \sqrt{\omega_0/\Gamma_0}$ the Markovian approximation is entirely broken.

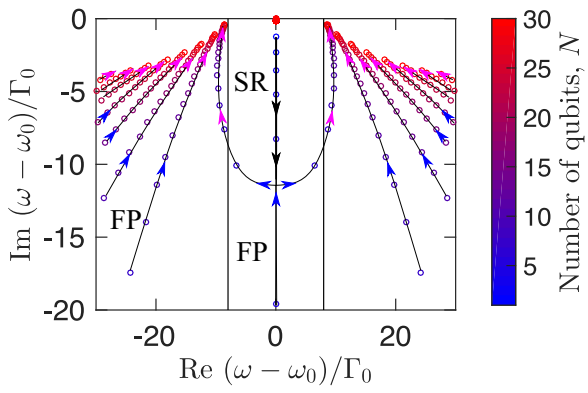

FIG. 6. Evolution of the complex energy spectrum of the Bragg qubit array with the number of qubits, N. Lines with arrows show the trajectories of Fabry-Pérot (FP) and superradiant (SR) modes with the increase of N. The calculation has been performed for $\Gamma_{\rm nonrad} = 0.2\Gamma_0$ and $\Gamma_0/\omega_0 = 10^{-2}$.

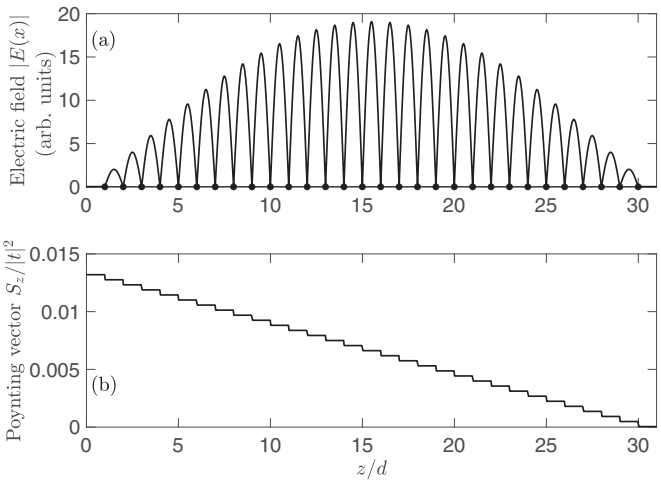

FIG. 7. (a) Electric field (9) calculated for the most subradiant mode of the 30-qubit array ($\omega - \omega_0 \approx -0.015\Gamma_0$). (b) Poynting vector (13) calculated for the structure excited from the left by the plane wave at the frequency ω_0. The Poynting vector has been normalized to the flux of the incident wave. The calculation has been performed for $\Gamma_{\rm nonrad} = 0.2\Gamma_0$ and $\Gamma_0/\omega_0 = 10^{-2}$.

The reflection coefficient for the infinite array can be obtained from Eq. (A9) taking the limit $N \to \infty$ and reads [23]

$$r_\infty(\omega) = \frac{1}{(\sqrt{w\tilde{w}} - \sqrt{w\tilde{w}-1})^2}, \tag{7}$$

where $w = (\omega - \omega_0)/\Delta$, $\tilde{w} = w + i\Gamma_{\rm nonrad}/\Delta$, $\Delta = \sqrt{2\Gamma_0\omega_0/\pi}$ is the half-width of the polariton band gap. The reflection coefficient (7) has four branching points, namely $\omega = \omega_0 \pm \Delta - i\Gamma/2$, $\omega = \omega_0$ and $\omega = \omega_0 - i\Gamma$. In the limit $N \to \infty$, the Fabry-Pérot modes accumulate near the band-gap edges in the points where $K(\omega)d = \pi$, as follows from Eq. (6). These points coincide with the two branching points of $r_\infty(\omega)$,

$$\omega_\pm = \omega_0 \pm \sqrt{\Delta^2 - \frac{\Gamma_{\rm nonrad}^2}{4}} - \frac{i\Gamma_{\rm nonrad}}{2}. \tag{8}$$

The decay rates of the Fabry-Pérot modes remain finite and tend to $-\,{\rm Im}\,\omega_\pm \equiv \Gamma_{\rm nonrad}/2$, half of the nonradiative decay rate of the qubits, reflecting the half-light half-qubit excitation nature of the polariton. The subradiant modes accumulate near the two other branching points $\omega = \omega_0$ and $\omega = \omega_0 - i\Gamma_{\rm nonrad}$.

B. Subradiant modes

To understand qualitatively the origin of the long lifetime of the most subradiant mode we plot in Fig. 7(a) the distribution of the electric field corresponding to the emission from the longest-living eigenmode for the array with $N = 30$ qubits. The electric field has been found as

$$E(z) = -i\sum_{m=1}^{N} e^{i\omega|z-md|/c}\psi_m, \tag{9}$$

where ψ_m is the eigenvector satisfying $H(\omega)\psi = \omega\psi$.

We have also calculated the Poynting vector for the 30-qubit array excited resonantly at the frequency $\omega = \omega_0$. To this end we have used the input-output theory in the formulation of Ref. [43], see also Ref. [44]. We first find the distribution of the qubit polarizations ψ_n induced by incident wave from

$$\sum_n H_{mn}(\omega_0)\psi_n = e^{im\omega_0 d/c}, \tag{10}$$

with $H_{mn}(\omega) = -i\delta_{mn}\Gamma_{\rm nonrad} - i\Gamma_0 e^{i\omega d|m-n|/c}$ and then calculate the distribution of electric and magnetic fields according to

$$E_x(z) = e^{i\omega z/c} - i\Gamma_0\sum_{m=1}^{N} e^{i\omega|z-md|/c}\psi_m, \tag{11}$$

$$H_y(z) = \frac{c}{i\omega}\frac{d}{dz}E_x. \tag{12}$$

The time-averaged Poynting vector is given by

$$S_z = \frac{c}{2\pi}\,{\rm Re}(E_x H_y^*), \tag{13}$$

where we assume that $E(t) = Ee^{-i\omega t} + {\rm c.c.}$

The calculated Poynting vector is shown in Fig. 7(b). The value of the Poynting vector has been normalized to that of the incident wave. It is constant between the qubits and exhibits small jumps at the qubit positions that reflect absorption of photons at the qubits. The total value of absorption for light incident at $\omega = \omega_0$ is given by [45]

$$A_N = \frac{2N\Gamma_{\rm nonrad}\Gamma_0}{(\Gamma_{\rm nonrad} + N\Gamma_0)^2}. \tag{14}$$

The absorption jump of the Poynting vector at each qubit is N times smaller, and approximately equal to $2\Gamma_{\rm nonrad}/(N^2\Gamma_0) \approx 5\times 10^{-4}$. This suppression of absorption at the qubit resonance can be seen as one of the manifestations of the Borrmann effect. In another words, since the reflection coefficient is almost unity, the electric field is almost a standing wave with nodes at the qubit positions.

IV. PERSISTENT QUANTUM CORRELATIONS

The uncovered long-lived modes pave the way for the long-lived quantum correlations in the Bragg qubit array, with the decay times longer than the nonradiative decay rate. To demonstrate this, we calculate the photon-photon correlation function $g^{(2)}(\tau) = \langle a^\dagger(0)a^\dagger(\tau)a(\tau)a(0)\rangle/\langle a^\dagger(0)a(0)\rangle$, where $a(t)$ is the photon destruction operator, for the light transmitted through the Bragg array under low-intensity coherent excitation at frequency ε. The correlations can be calculated by using the known solution for the wave function, describing a scattering of a photon pair on array of qubits that has the form [46,47]:

$$\psi_2 = t^{\dagger,2}a^\dagger_{\varepsilon/c}a^\dagger_{\varepsilon/c}|0\rangle + \frac{i}{2}\int_{-\infty}^{\infty}\frac{d\omega}{2\pi}M(\varepsilon+\omega,\varepsilon-\omega)a^\dagger_{\varepsilon-\omega}a^\dagger_{\varepsilon+\omega}|0\rangle. \tag{15}$$

Here, the first term describes an independent transmission of the photon pair with the transmission coefficient $t = 1 + i\Gamma_0\sum_{m,n=1}^{N} G_{mn}(\varepsilon)e^{i\varepsilon(z_m+z_n)/c}$. The second term describes an

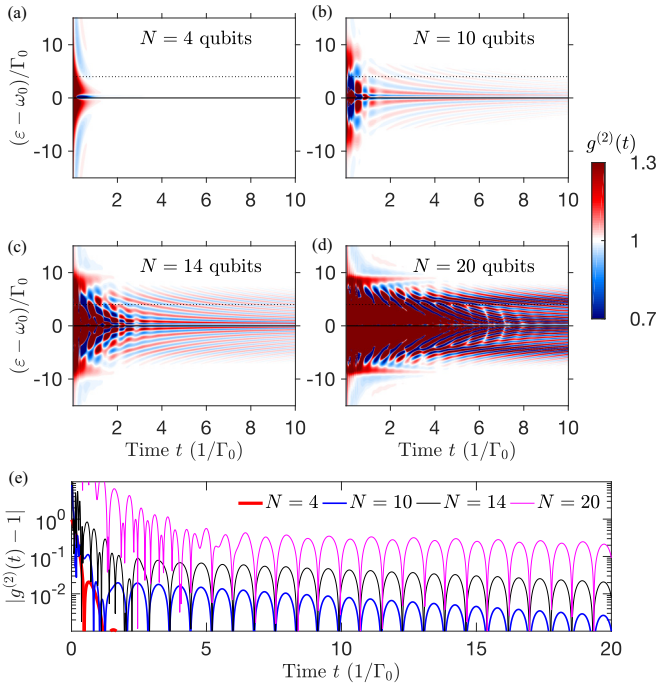

FIG. 8. (a)–(d) Time dependence of photon-photon correlations $g^{(2)}(t)$ scanned vs the energy of incoming photons ε calculated for the Bragg array with $N = 4$, 10, 14, 20 qubits. Panel (e) shows the time dynamics for at $\varepsilon - \omega_0 = 4\Gamma_0$ [dotted line in panels (a)–(d)]. The other parameters are the same as in Fig. 2.

incoherent-scattering process with transmission of two photons with the energies $\varepsilon - \omega$ and $\varepsilon + \omega$. The scattering matrix $M(\varepsilon + \omega, \varepsilon - \omega)$ is found following Zheng and Baranger [31], see also Ref. [48]:

$$M(\omega_1', \omega_2') = -2i\Gamma_0^2 \sum_{m,n=1}^{N} s_n^-(\omega_1') s_n^-(\omega_2') Q_{nm} s_m^+(\varepsilon) s_m^+(\varepsilon), \tag{16}$$

with $s_m^{\pm}(\omega) = \sum_m G_{mn} e^{\pm i(\omega/c)z_n}$ and $Q_{nm} = [\Sigma^{-1}]_{nm}$, $\Sigma_{nm} = \int d\omega G_{nm}(\omega) G_{nm}(2\varepsilon - \omega)/(2\pi)$. Here the kernel Q describes the so-called two-photon bound-state resonance [46]. Calculating the photon-photon correlations using the wave function ψ_2 as $\langle \psi_2 | a^\dagger(0) a^\dagger(\tau) a(\tau) a(0) | \psi_2 \rangle$ we obtain [36]

$$g^{(2)}(\tau, \varepsilon) = \left| 1 + \frac{i}{2t^2(\varepsilon)} \int_{-\infty}^{\infty} \frac{d\omega}{2\pi} e^{-i\omega\tau} M(\varepsilon + \omega, \varepsilon - \omega) \right|^2. \tag{17}$$

The details of the evaluation of the integral over ω are presented in Appendix B.

Figure 8 shows the time dependence $g^{(2)}(\tau)$ obtained numerically for different incident light frequencies ε and array lengths $N = 4$, 10, 14, 20. At relatively short times the function $g^{(2)}(\tau)$ demonstrates strong photon bunching when the excitation frequency ε is close to ω_0. The single-photon transmittance $|t(\omega_0)|^2$ is suppressed in the vicinity of resonance due to the strong reflection, so that photons can pass through the structure only in pairs. The calculation demonstrates that photon-photon correlations strongly depend on the number of qubits N. The changes are most prominent for small N, reflecting the breakdown of the Markovian approximation and the superradiant regime. For a short structure with $N = 4$ [Fig. 8(a)], in the wide spectral range $\Gamma_0 \lesssim |\varepsilon - \omega_0| \lesssim N\Gamma_0$, the function $g^{(2)}(\tau)$ rapidly decays to 1 at the timescale of the superradiant mode, $\approx 1/(N\Gamma_0)$. In long structures, Figs. 8(c) and 8(d), the decay is nonmonotonic and the correlations oscillate with time. At large times the correlation function oscillates with frequency and can be both larger than unity (red areas, photon bunching) and smaller than unity (blue areas, photon antibunching). Strong photon bunching is observed when the excitation energy is close to the edges of the polariton band gap $\omega_0 \pm \Delta \approx \omega_0 \pm 8\Gamma_0$. Crucially, the decay of the correlations becomes significantly slower for larger N. This is also seen from Fig. 8(e), showing the dynamics of the correlations for the particular excitation energy $\varepsilon = \omega_0 + 4\Gamma_0 \approx \omega_0 + \Delta/2$ when the amplitude of the correlations at large times is at a maximum. This energy corresponds to the regime of photon-photon interaction when one of the two scattered photons is at the resonance with the Fabry-Pérot mode near the polariton band-gap edge $\omega_0 + \Delta$ and at the same time the other photon is at the resonance with the subradiant states with $\mathrm{Re}\,\omega = \omega_0$. The lifetime of the correlations is longer than both radiative and nonradiative lifetimes of a single qubit $t_{\mathrm{rad}} = 1/(2\Gamma_0)$ and $t_{\mathrm{nonrad}} = 5t_{\mathrm{rad}}$ for the parameters of Fig. 8. We have calculated the lifetime of correlations and plotted it by blue open circles in Fig. 2(a). The calculation agrees with Eq. (5) (black line): the lifetime grows for longer arrays as N^2. Since $\min(\mathrm{Im}\,\omega) \to 0$ for $N \to \infty$, we expect slow nonexponential power-law decay in the limit of infinite structure.

V. SUMMARY

To summarize, we predict that photon-photon correlations become partially immune from nonradiative dissipation due to the Borrmann effect, when the light wave has nodes at the qubit positions. Our results demonstrate that the properties of the Bragg-spaced array of qubits, when $\omega_0 d/c = \pi, 2\pi, \ldots$ are strongly different from those in the conventional metamaterial regime when $\omega_0 d/c \ll \pi$ [14]. Thus, Bragg-spaced arrays offer new possibilities to manipulate the quantum light. While the studied time dynamics probes only the lifetimes of single-excited states, novel physics can be expected for the double-excited states. The interaction-induced localization and topological transitions have been recently predicted for two-polariton states [49,50], but the non-Markovian regime of polariton-polariton interactions remains fully unexplored. For instance, one can imagine a situation when a pass-band of bound two-polariton states [51,52] forms within a single-polariton Bragg stop-band, leading to the highly selective two-photon transmission. Novel opportunities are also opened by the two-dimensional arrays of atoms [53–55], which have recently become available [30].

ACKNOWLEDGMENTS

We acknowledge numerous useful discussions with E. L. Ivchenko. This work was supported by the Russian President Grant No. MD-243.2020.2 and the Russian foundation for Basic Research Grant No. 18-29-20037. Analytical calculation of the single-photon energy spectrum was funded by the Russian Science Foundation Project No. 20-12-00194.

APPENDIX A: OPTICAL SPECTRA AND LIFETIME OF MOST SUBRADIANT MODE

In this Appendix we derive Eq. (5) from the main text for the lifetime of the longest-living mode in the qubit array. It can be obtained from the complex resonance frequency of the amplitude reflection coefficient of light from the array of qubits. The corresponding expressions for reflection coefficient have been known at least since 1994 when a theory of light reflection from periodic array of semiconductor quantum wells [20,45,56] was developed. Quite a similar problem of light interacting with resonance scatterers was also considered much earlier in the context of resonant γ-ray diffraction on the nuclei in crystals. Such crystals have been experimentally studied since the 1960s, see reviews [18,57] for more details. Some other examples of resonant scatterers where the same equations are valid include ring resonators [58], metallic gratings with plasmonic resonances [3], and dielectric cylinders with Mie resonances [59]. A detailed comparison between cold atom systems, semiconductor lattices, and Mössbauer isotopes can be found in the review [24]. Very recently, it was also theoretically proposed to consider Bragg lattices of superconducting qubits coupled to the waveguide [60] where the expressions equivalent to those in Ref. [20] have been obtained.

To derive reflection and transmission coefficients one can use the transfer-matrix technique. The electric field to the left and right of the qubit, located at the point $z = 0$, is presented as

$$E(z) = \begin{cases} E_L^{\rightarrow} e^{i\omega z/c} + E_L^{\leftarrow} e^{-i\omega z/c} & (z < 0) \\ E_R^{\rightarrow} e^{i\omega z/c} + E_R^{\leftarrow} e^{-i\omega z/c} & (z > 0) \end{cases} \tag{A1}$$

(we assume the $e^{-i\omega t}$ time dependence). The fields to the left and right of the atom are linked as [20,26]

$$\begin{pmatrix} E_R^{\rightarrow} \\ E_R^{\leftarrow} \end{pmatrix} = M_0 \begin{pmatrix} E_L^{\rightarrow} \\ E_L^{\leftarrow} \end{pmatrix} \tag{A2}$$

by the transfer matrix

$$M_0 = \frac{1}{t} \begin{pmatrix} t^2 - r^2 & r \\ -r & 1 \end{pmatrix}, \tag{A3}$$

where the reflection and transmission for a single qubit are [61]

$$r = \frac{i\Gamma_0}{\omega_0 - \omega - i(\Gamma_{\text{nonrad}} + \Gamma_0)}, \tag{A4}$$

$$t = 1 + r = \frac{\omega_0 - \omega}{\omega_0 - \omega - i(\Gamma_{\text{nonrad}} + \Gamma_0)}. \tag{A5}$$

The total transfer matrix through an array of N qubits with the period d is given by

$$M_N = (M_d M_0)^N, \tag{A6}$$

where the transfer matrix through the free part of the waveguide with the length d is

$$M_d = \begin{pmatrix} e^{i\omega d/c} & 0 \\ 0 & e^{-i\omega d/c} \end{pmatrix}. \tag{A7}$$

The array reflection and transmission coefficients are given by

$$r_N = -\frac{[M_N]_{2,1}}{[M_N]_{2,2}}, \quad t_N = -\frac{\det M_N}{[M_N]_{2,2}}. \tag{A8}$$

It is also possible to obtain an analytical expression for Eqs. (A8) that reads [24,62]

$$r_N = \frac{\tilde{r} \sin NKd}{\sin NKd - \tilde{t} \sin(N-1)Kd},$$

$$t_N = \frac{\tilde{t} \sin Kd}{\sin NKd - \tilde{t} \sin(N-1)Kd}, \tag{A9}$$

where $\tilde{t} = te^{i\omega d/c}$, $\tilde{r} = re^{i\omega d/c}$ are the transmission and reflection coefficients through one period of the array and the Bloch wave vector $K(\omega)$ is determined by the dispersion of polaritonic excitations, propagating in the array

$$\cos Kd = \frac{1}{2} \text{Tr}(M_{\text{atom}} M_{\text{period}}) = \cos\frac{\omega d}{c} - \frac{\Gamma_0}{\omega_0 - \omega - i\Gamma_{\text{nonrad}}} \sin\frac{\omega d}{c}. \tag{A10}$$

In the considered Bragg structure, where $\omega_0 d/c = \pi$, we have $|Kd - \pi| \ll 1$ in the vicinity of exciton resonance and the polariton dispersion can be simplified to [24]

$$\frac{Kd}{\pi} - 1 = \pm\sqrt{\left(\frac{\omega - \omega_0}{\omega_0}\right)^2 - \left(\frac{\Delta}{\omega_0}\right)^2 \frac{\omega - \omega_0}{\omega - \omega_0 + i\Gamma_{\text{nonrad}}}}, \tag{A11}$$

where $\Delta = \sqrt{2\Gamma_0 \omega_0/\pi}$ is the half-width of the Bragg band gap [45,56]. The dispersion law (A10) and the reflection and transmission coefficients are plotted in Fig. 5. The calculation demonstrates a polariton Bragg band gap in the range $(\omega_0 - \Delta,\ \omega_0 + \Delta)$ where $\Delta \approx 8\Gamma_0$ for the parameters of the system. The specific feature of the Bragg array is that the band gap width 2Δ exceeds the radiative linewidth of a single qubit Γ_0 by a large factor $\sim\sqrt{\omega_0/\Gamma_0}$. The explicit solution for the Green's function for arbitrary number of qubits is given in Ref. [63].

To find the eigenfrequencies of the subradiant modes we solve the equation

$$\sin NKd - \tilde{t} \sin(N-1)Kd = 0 \tag{A12}$$

for a zero of the denominator of the reflection coefficient (A9) using approximate (A11) for the polariton dispersion. We take into account that, for the considered subradiant, eigenmodes $\text{Re}\,\omega = \omega_0$ and $|\text{Im}\,\omega| \sim \Gamma_0 \ll \Delta$. Comparison with numerical calculation shows that the darkest subradiant mode approximately satisfies the interference condition,

$$NK(\omega)d = \pi, \tag{A13}$$

which is a usual condition for a standing wave in a finite structure. Indeed, given Eq. (A13) both sine factors in Eq. (A12) turn to zero. To solve Eq. (A13) for ω we notice that for $|\omega - \omega_0| \ll \omega_0$ the first term under the square root in Eq. (A11) can be neglected. As a result, we obtain a simple algebraic equation for ω. Solving it and calculating the imaginary part of ω, $1/t = -2\,\text{Im}\,\omega$, we get Eq. (5) from the main text.

We also note the presence of a resonant feature in the polariton dispersion and in the reflection spectrum in the center

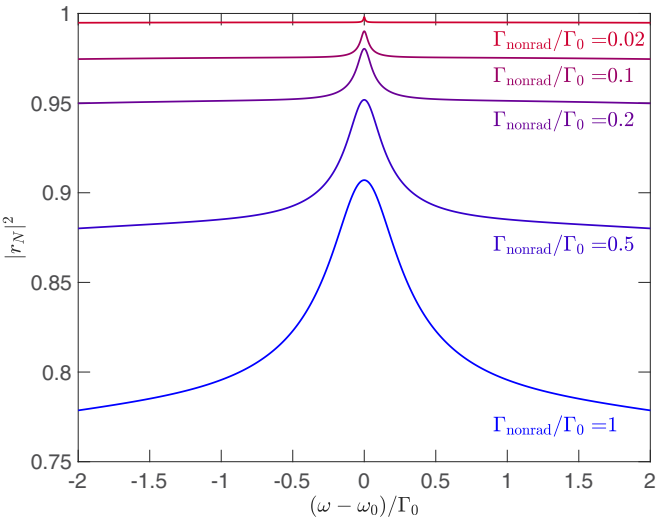

FIG. 9. Reflection spectra in the vicinity of the qubit resonance frequency ω_0 depending on the nonradiative decay rate $\Gamma_{\rm nonrad}$ indicated near each curve. The calculation has been performed for $N = 20$ qubits and $\Gamma_0/\omega_0 = 10^{-2}$.

of the band gap at $\omega = \omega_0$. This feature is related to excitation of subradiant modes in the system. We show in Fig. 9 the evolution of the reflection spectra $|r_N|^2$ in the vicinity of the qubit resonance frequency $\omega = \omega_0$ depending on the nonradiative decay rate of a single qubit $\Gamma_{\rm nonrad}$. For $\Gamma_{\rm nonrad} = 0.02\Gamma_0$ (red curve), the reflection coefficient is close to unity over the entire plotted range. This is because of the presence of the Bragg band gap in the polariton spectrum in the range $\omega_0 - \Delta \ldots \omega_0 + \Delta$ where $\Delta = \sqrt{2\Gamma_0\omega_0/\pi} \approx 8\Gamma_0$. When the nonradiative decay rate increases, the reflection coefficient in the entire band gap is suppressed except for the narrow feature with a linewidth $\approx\Gamma$ at the qubit resonance. This narrow resonant feature, surviving the nonradiative decay, is a manifestation of the Borrmann effect discussed in the main text. It results from a resonant excitation of the subradiant modes.

APPENDIX B: CALCULATION OF PHOTON-PHOTON CORRELATION FUNCTION

In this Appendix we provide more information on the evaluation of the integral

$$\int_{-\infty}^{\infty} \frac{d\omega}{2\pi} e^{-i\omega\tau} M(\varepsilon+\omega, \varepsilon-\omega) \tag{B1}$$

entering the photon-photon correlation function (9) in the main text. Recall the definitions of the relevant quantities below. The scattering matrix is

$$M(\omega_1', \omega_2') = -2i\Gamma_0^2 \sum_{m,n=1}^{N} s_n^-(\omega_1') s_n^-(\omega_2') Q_{nm} s_m^+(\varepsilon) s_m^+(\varepsilon), \tag{B2}$$

with

$$s_m^{\pm}(\omega) = \sum_m G_{mn} e^{\pm i(\omega/c)z_n}, \tag{B3}$$

$Q_{nm} = [\Sigma^{-1}]_{nm}$, $\Sigma_{nm} = \int d\omega G_{nm}(\omega) G_{nm}(2\varepsilon - \omega)/(2\pi)$, and the Green's function is defined by the equation

$$G(\omega) = [H(\omega) - \omega]^{-1}, \tag{B4}$$

with

$$H_{mn}(\omega) = (\omega_0 - i\Gamma_{\rm nonrad})\delta_{mn} - i\Gamma_0 e^{i\omega|z_m - z_n|/c}. \tag{B5}$$

The integration over ω in Eq. (B1) in the non-Markovian regime requires some care due to the presence of factors $e^{\pm i(\omega/c)z_n}$ in Eqs. (B3) for $s^{\pm}$. In the Markovian approximation one could replace $e^{\pm i(\omega/c)z_n}$ in Eqs. (B3) by $e^{\pm i(\omega_0/c)z_n}$ and $H(\omega)$ in Eq. (B4) by $H(\omega_0)$ and then use the Cauchy integration formula directly. In the non-Markovian regime we first get rid of the ω dependence in the factors $e^{\pm i(\omega/c)z_n}$ in $s_m^{\pm}(\omega)$ by using

$$s_m^{\pm}(\omega) = -\frac{e^{i(\omega/c)z_{n^{\pm}}}}{i\Gamma_0}[\delta_{m,n^{\pm}} + (\omega - \omega_0 + i\Gamma)G_{m,n^{\pm}}], \tag{B6}$$

where $n^+ = 1$, $n^- = N$ that follows from the Green's function definition Eq. (B4). The advantage of the representation Eq. (B6) is that the factor $e^{i(\omega/c)z_{n^{\pm}}}$ is the same for all $s_m^{\pm}$. As such, it can be eliminated by a suitable choice of the coordinate.

Next, we expand the Green's function as

$$G_{mn} = \sum_{\nu} \frac{g_{mn}^{\nu}}{\omega_{\nu} - \omega}, \tag{B7}$$

where ω_{ν} are the eigenfrequencies of the Hamiltonian (4). We find these eigenfrequencies numerically within some large finite region in the complex around the frequency ω_0 with the size on the order of $100\Gamma_0$. and the residue matrices g_{mn}^{ν} are determined following Ref. [64]. Finally, using the sum rule $\sum_{\nu} g_{mn}^{\nu} = \delta_{mn}$, we find

$$s_m^{\pm} = \sum_{\nu} \frac{s_m^{\nu,\pm}}{\omega_{\nu} - \omega}, \quad s_m^{\nu,\pm} = ie^{i(\omega/c)z_{n^{\pm}}} g_{m,n^{\pm}}^{\nu} \frac{\omega_{\nu} - \omega_0 + i\Gamma}{\Gamma_0}.$$

After this expansion is substituted into Eq. (B2) the only dependence on ω would be in the resonance terms $\propto 1/(\omega_{\nu} - \omega)$. Next, we use the Cauchy integration formula to obtain the two-photon correlations in the form

$$g^{(2)}(\tau) = \left| 1 - i \sum_{\nu\mu} \sum_{m,n=1}^{N} \frac{s_n^{\nu,+} s_n^{\mu,+} e^{-i\omega_{\nu}\tau + i\varepsilon\tau} M_{nm}(\varepsilon) s_m^+(\varepsilon) s_m^+(\varepsilon)}{t(\varepsilon)^2 (2\varepsilon - \omega_{\nu} - \omega_{\mu})} \right|^2. \tag{B8}$$

[1] D. E. Chang, J. S. Douglas, A. González-Tudela, C.-L. Hung, and H. J. Kimble, Colloquium: quantum matter built from nanoscopic lattices of atoms and photons, Rev. Mod. Phys. **90**, 031002 (2018).

[2] M. F. Limonov, M. V. Rybin, A. N. Poddubny, and Y. S. Kivshar, Fano resonances in photonics, Nat. Photonics **11**, 543 (2017).

[3] R. Taubert, D. Dregely, T. Stroucken, A. Christ, and H. Giessen, Octave-wide photonic band gap in three-dimensional plasmonic Bragg structures and limitations of radiative coupling, Nat. Commun. **3**, 691 (2012).

[4] A. I. Kuznetsov, A. E. Miroshnichenko, M. L. Brongersma, Y. S. Kivshar, and B. Luk'yanchuk, Optically resonant dielectric nanostructures, Science **354**, aag2472 (2016).

[5] N. S. Averkiev, M. M. Glazov, and A. N. Poddubnyi, Collective modes of quantum dot ensembles in microcavities, J. Exp. Theor. Phys. **108**, 836 (2009).

[6] H. Gibbs, G. Khitrova, and S. Koch, Exciton-polariton light-semiconductor coupling effects, Nat. Photonics **5**, 273 (2011).

[7] C. W. Hsu, B. Zhen, A. D. Stone, J. D. Joannopoulos, and M. Soljačić, Bound states in the continuum, Nat. Rev. Mater. **1**, 16048 (2016).

[8] K. Koshelev, S. Kruk, E. Melik-Gaykazyan, J.-H. Choi, A. Bogdanov, H.-G. Park, and Y. Kivshar, Subwavelength dielectric resonators for nonlinear nanophotonics, Science **367**, 288 (2020).

[9] D. E. Chang, L. Jiang, A. V. Gorshkov, and H. J. Kimble, Cavity QED with atomic mirrors, New J. Phys. **14**, 063003 (2012).

[10] L. Ostermann, C. Meignant, C. Genes, and H. Ritsch, Super- and subradiance of clock atoms in multimode optical waveguides, New J. Phys. **21**, 025004 (2019).

[11] Y.-X. Zhang and K. Mølmer, Theory of Subradiant States of a One-Dimensional Two-Level Atom Chain, Phys. Rev. Lett. **122**, 203605 (2019).

[12] Y. Ke, A. V. Poshakinskiy, C. Lee, Y. S. Kivshar, and A. N. Poddubny, Inelastic Scattering of Photon Pairs in Qubit Arrays with Subradiant States, Phys. Rev. Lett. **123**, 253601 (2019).

[13] A. N. Poddubny, Quasiflat band enabling subradiant two-photon bound states, Phys. Rev. A **101**, 043845 (2020).

[14] J. D. Brehm, A. N. Poddubny, A. Stehli, T. Wolz, H. Rotzinger, and A. V. Ustinov, Waveguide bandgap engineering with an array of superconducting qubits, npj Quantum Mater. **6**, 10 (2021).

[15] G. Borrmann, Uber Extinktionsdiagramme von Quartz, Physikal. Zeit. **42**, 157 (1941).

[16] G. Borrmann, Die Absorption von Röntgenstrahlen im Fall der Interferenz, Zeitschrift für Physik **127**, 297 (1950).

[17] A. M. Afanas'ev and Y. Kagan, Suppression of inelastic channels in resonant nuclear scattering in crystals, JETP **21**, 215 (1965).

[18] Y. Kagan, Theory of coherent phenomena and fundamentals in nuclear resonant scattering, Hyperfine Interact. **123**, 83 (1999).

[19] V. B. Novikov and T. V. Murzina, Borrmann effect in Laue diffraction in one-dimensional photonic crystals under a topological phase transition, Phys. Rev. B **99**, 245403 (2019).

[20] E. L. Ivchenko, A. I. Nesvizhskii, and S. Jorda, Bragg reflection of light from quantum-well structures, Phys. Solid State **36**, 1156 (1994).

[21] M. Hübner, J. Kuhl, T. Stroucken, A. Knorr, S. W. Koch, R. Hey, and K. Ploog, Collective Effects of Excitons in Multiple-Quantum-Well Bragg and Anti-Bragg Structures, Phys. Rev. Lett. **76**, 4199 (1996).

[22] D. Goldberg, L. I. Deych, A. A. Lisyansky, Z. Shi, V. M. Menon, V. Tokranov, M. Yakimov, and S. Oktyabrsky, Exciton-lattice polaritons in multiple-quantum-well-based photonic crystals, Nat. Photonics **3**, 662 (2009).

[23] A. V. Poshakinskiy, A. N. Poddubny, and S. A. Tarasenko, Reflection of short polarized optical pulses from periodic and aperiodic multiple quantum well structures, Phys. Rev. B **86**, 205304 (2012).

[24] A. Poddubny and E. Ivchenko, Resonant diffraction of electromagnetic waves from solids (a review), Phys. Solid State **55**, 905 (2013).

[25] J. D. Joannopoulos, S. G. Johnson, J. N. Winn, and R. D. Meade, *Photonic Crystals: Molding the Flow of Light* (Princeton University Press, Princeton, 2008) .

[26] N. V. Corzo, B. Gouraud, A. Chandra, A. Goban, A. S. Sheremet, D. V. Kupriyanov, and J. Laurat, Large Bragg Reflection from One-Dimensional Chains of Trapped Atoms Near a Nanoscale Waveguide, Phys. Rev. Lett. **117**, 133603 (2016).

[27] H. L. Sørensen, J.-B. Béguin, K. W. Kluge, I. Iakoupov, A. S. Sørensen, J. H. Müller, E. S. Polzik, and J. Appel, Coherent Backscattering of Light Off One-Dimensional Atomic Strings, Phys. Rev. Lett. **117**, 133604 (2016).

[28] N. V. Corzo, J. Raskop, A. Chandra, A. S. Sheremet, B. Gouraud, and J. Laurat, Waveguide-coupled single collective excitation of atomic arrays, Nature (London) **566**, 359 (2019).

[29] M. Mirhosseini, E. Kim, X. Zhang, A. Sipahigil, P. B. Dieterle, A. J. Keller, A. Asenjo-Garcia, D. E. Chang, and O. Painter, Cavity quantum electrodynamics with atom-like mirrors, Nature (London) **569**, 692 (2019).

[30] J. Rui, D. Wei, A. Rubio-Abadal, S. Hollerith, J. Zeiher, D. M. Stamper-Kurn, C. Gross, and I. Bloch, A subradiant optical mirror formed by a single structured atomic layer, Nature (London) **583**, 369 (2020).

[31] H. Zheng and H. U. Baranger, Persistent Quantum Beats and Long-Distance Entanglement from Waveguide-Mediated Interactions, Phys. Rev. Lett. **110**, 113601 (2013).

[32] A. Sipahigil, R. E. Evans, D. D. Sukachev, M. J. Burek, J. Borregaard, M. K. Bhaskar, C. T. Nguyen, J. L. Pacheco, H. A. Atikian, C. Meuwly, R. M. Camacho, F. Jelezko, E. Bielejec, H. Park, M. Lončar, and M. D. Lukin, An integrated diamond nanophotonics platform for quantum-optical networks, Science **354**, 847 (2016).

[33] A. P. Foster, D. Hallett, I. V. Iorsh, S. J. Sheldon, M. R. Godsland, B. Royall, E. Clarke, I. A. Shelykh, A. M. Fox, M. S. Skolnick, I. E. Itskevich, and L. R. Wilson, Tunable Photon Statistics Exploiting the Fano Effect in a Waveguide, Phys. Rev. Lett. **122**, 173603 (2019).

[34] S. Mahmoodian, G. Calajó, D. E. Chang, K. Hammerer, and A. S. Sørensen, Dynamics of Many-Body Photon Bound States in Chiral Waveguide QED, Phys. Rev. X **10**, 031011 (2020).

[35] A. S. Prasad, J. Hinney, S. Mahmoodian, K. Hammerer, S. Rind, P. Schneeweiss, A. S. Sørensen, J. Volz, and A. Rauschenbeutel, Correlating photons using the collective nonlinear response of atoms weakly coupled to an optical mode, Nat. Photonics **14**, 719 (2020).

[36] A. V. Poshakinskiy and A. N. Poddubny, Biexciton-mediated superradiant photon blockade, Phys. Rev. A **93**, 033856 (2016).

[37] A. A. Abrikosov, Electron scattering on magnetic impurities in metals and anomalous resistivity effects, Phys. Phys. Fiz. **2**, 5 (1965).

[38] T. Caneva, M. T. Manzoni, T. Shi, J. S. Douglas, J. I. Cirac, and D. E. Chang, Quantum dynamics of propagating photons with strong interactions: A generalized input–output formalism, New J. Phys. **17**, 113001 (2015).

[39] J. J. Burnett, A. Bengtsson, M. Scigliuzzo, D. Niepce, M. Kudra, P. Delsing, and J. Bylander, Decoherence benchmarking of superconducting qubits, npj Quantum Inf. **5**, 54 (2019).

[40] D. F. Kornovan, A. S. Sheremet, and M. I. Petrov, Collective polaritonic modes in an array of two-level quantum emitters coupled to an optical nanofiber, Phys. Rev. B **94**, 245416 (2016).

[41] V. A. Pivovarov, A. S. Sheremet, L. V. Gerasimov, J. Laurat, and D. V. Kupriyanov, Quantum interface between light and a one-dimensional atomic system, Phys. Rev. A **101**, 053858 (2020).

[42] V. A. Kiselev, B. S. Razbirin, and I. N. Uraltsev, Additional waves and Fabry-Perot interference of photoexcitons (polaritons) in thin II–VI crystals, Phys. Status Solidi B **72**, 161 (1975).

[43] V. A. Kosobukin and A. N. Poddubny, Exciton-polariton absorption in periodic and disordered quantum-well chains, Phys. Solid State **49**, 1977 (2007).

[44] W. Suh, Z. Wang, and S. Fan, Temporal coupled-mode theory and the presence of non-orthogonal modes in lossless multimode cavities, IEEE J. Quantum Electron. **40**, 1511 (2004).

[45] M. M. Voronov, E. L. Ivchenko, V. A. Kosobukin, and A. N. Poddubny, Specific features in reflectance and absorbance spectra of one-dimensional resonant photonic crystals, Phys. Solid State **49**, 1792 (2007).

[46] J.-T. Shen and S. Fan, Strongly correlated multiparticle transport in one dimension through a quantum impurity, Phys. Rev. A **76**, 062709 (2007).

[47] V. I. Yudson and P. Reineker, Multiphoton scattering in a one-dimensional waveguide with resonant atoms, Phys. Rev. A **78**, 052713 (2008).

[48] M. Laakso and M. Pletyukhov, Scattering of Two Photons from Two Distant Qubits: Exact Solution, Phys. Rev. Lett. **113**, 183601 (2014).

[49] J. Zhong, N. A. Olekhno, Y. Ke, A. V. Poshakinskiy, C. Lee, Y. S. Kivshar, and A. N. Poddubny, Photon-Mediated Localization in Two-Level Qubit Arrays, Phys. Rev. Lett. **124**, 093604 (2020).

[50] A. V. Poshakinskiy, J. Zhong, Y. Ke, N. A. Olekhno, C. Lee, Y. S. Kivshar, and A. N. Poddubny, Quantum Hall phases emerging from atom–photon interactions, npj Quantum Inf. **7**, 34 (2021).

[51] Y.-X. Zhang, C. Yu, and K. Mølmer, Subradiant bound dimer excited states of emitter chains coupled to a one dimensional waveguide, Phys. Rev. Research **2**, 013173 (2020).

[52] Z. Wang, T. Jaako, P. Kirton, and P. Rabl, Supercorrelated Radiance in Nonlinear Photonic Waveguides, Phys. Rev. Lett. **124**, 213601 (2020).

[53] R. J. Bettles, S. A. Gardiner, and C. S. Adams, Enhanced Optical Cross Section Via Collective Coupling of Atomic Dipoles in a 2D Array, Phys. Rev. Lett. **116**, 103602 (2016).

[54] G. Facchinetti, S. D. Jenkins, and J. Ruostekoski, Storing Light with Subradiant Correlations in Arrays of Atoms, Phys. Rev. Lett. **117**, 243601 (2016).

[55] E. Shahmoon, D. S. Wild, M. D. Lukin, and S. F. Yelin, Cooperative Resonances in Light Scattering from Two-Dimensional Atomic Arrays, Phys. Rev. Lett. **118**, 113601 (2017).

[56] L. I. Deych and A. A. Lisyansky, Polariton dispersion law in periodic-Bragg and near-Bragg multiple quantum well structures, Phys. Rev. B **62**, 4242 (2000).

[57] J. Hannon and G. Trammell, Coherent γ-ray optics, Hyperfine Interact. **123**, 127 (1999).

[58] M. F. Yanik, W. Suh, Z. Wang, and S. Fan, Stopping Light in a Waveguide with an All-Optical Analog of Electromagnetically Induced Transparency, Phys. Rev. Lett. **93**, 233903 (2004).

[59] M. V. Rybin, D. S. Filonov, K. B. Samusev, P. A. Belov, Y. S. Kivshar, and M. F. Limonov, Phase diagram for the transition from photonic crystals to dielectric metamaterials, Nat. Commun. **6**, 10102 (2015).

[60] Y. S. Greenberg, A. A. Shtygashev, and A. G. Moiseev, Waveguide band-gap N-qubit array with a tunable transparency resonance, Phys. Rev. A **103**, 023508 (2021).

[61] O. Astafiev, A. M. Zagoskin, A. A. Abdumalikov, Y. A. Pashkin, T. Yamamoto, K. Inomata, Y. Nakamura, and J. S. Tsai, Resonance fluorescence of a single artificial atom, Science **327**, 840 (2010).

[62] E. L. Ivchenko, *Optical Spectroscopy of Semiconductor Nanostructures* (Alpha Science International, Harrow, 2005) .

[63] M. Voronov, E. Ivchenko, M. Erementchouk, L. Deych, and A. Lisyansky, Photoluminescence spectroscopy of one-dimensional resonant photonic crystals, J. Lumin. **125**, 112 (2007).

[64] N. A. Gippius and S. G. Tikhodeev, Application of the scattering matrix method for calculating the optical properties of metamaterials, Phys. Usp. **52**, 967 (2009).